# Beach slopes from satellite-derived shorelines

**Kilian Vos[1], Mitchell D. Harley[1], Kristen D. Splinter[1], Andrew Walker[1], Ian L. Turner[1]**

[1] Water Research Laboratory, School of Civil and Environmental Engineering, UNSW Sydney, 110 King Street, Manly Vale, NSW 2093, Australia

Corresponding author: Kilian Vos (k.vos@unsw.edu.au)

**Key Points [140 characters each]:**

- Novel technique to estimate beach-face slopes from satellite imagery and modelled tides, removing the need for any *in situ* observations.
- Time-series of shoreline change are transformed into frequency domain to find the slope that minimises high-frequency tidal fluctuations.
- Beach-face slopes estimated at 1000's of beaches in eastern Australia and California USA reveal a similar regional-scale distribution.

**Abstract [150 words]**

The steepness of the beach face is a fundamental parameter for coastal morphodynamic research. Despite its importance, it remains extremely difficult to obtain reliable estimates of the beach-face slope over large spatial scales (1000's of km of coastline). In this letter, a novel approach to estimate this slope from time-series of satellite-derived shoreline positions is presented. This new technique uses a frequency-domain analysis to find the optimum slope that minimises high-frequency tidal fluctuations relative to lower-frequency erosion/accretion signals. A detailed assessment of this new approach at 8 locations spanning a range of tidal regimes, wave climates and sediment grain sizes shows strong agreement ($R^2$ = 0.9) with field measurements. The automated technique is then applied across 1000's of beaches in eastern Australia and California USA, revealing similar regional-scale distributions along these two contrasting coastlines and highlights the potential for new global-scale insight to beach-face slope spatial distribution, variability and trends.

**Plain Language Summary [Optional]**

How steep a beach is can dictate the way the beach interacts with the incoming ocean waves and therefore is of paramount importance for coastal scientists and engineers, coastal flood modelers and swim-safety officers. However, despite its importance, it is impractical to obtain reliable estimates of the 'typical' beach-face slope along large lengths of sandy coastlines (100's to 1000's of km) because of the logistics that would be necessary to visit many sites repeatedly to obtain these measurements. In this letter, we describe a new technique to estimate the beach-face slope in the absence of field observations, relying instead on long-term publicly available satellite observations and a global tide model. This technique is then applied to 1000's of beaches along the coastlines of eastern Australia and California in the USA.

## 1 Introduction

The beach face is the most seaward region of the subaerial beach, where remaining ocean wave energy, following dissipation across the surf zone, is converted to potential energy in the form of wave runup and setup (Stockdon et al., 2006). The steepness of the beach face is closely related to grain size (Bujan et al., 2019), with gravel beaches typically adopting a steeper beach face ($\tan\beta > 0.1$) and finer sand beaches a flatter beach face ($\tan\beta \sim 0.01$-$0.1$). It is one of the key parameters controlling the elevation of wave runup and total swash excursion at the shoreline, processes that are of primary concern for assessing coastal inundation hazards along the coastal boundary (Senechal et al., 2011; Stockdon et al., 2007). The beach-face slope is also a useful proxy for surf zone morphology (Harley et al., 2015), which in the absence of difficult-to-obtain surf-zone bathymetric measurements, can inform surf-zone hydrodynamics (Battjes, 1974) such as wave breaker type (i.e., spilling, plunging or surging waves), wave set-up across the surf zone (Stephens et al., 2011) as well as beach swimmer safety (Short et al., 1993).

While the beach-face slope can be readily measured at individual beaches using conventional survey techniques, beach-face slope estimates at large spatial scales (i.e., regional, national or

global) has to-date remained a core challenge. A key limitation is that remote sensing methods needed to collect data at such scale – for instance UAV-based structure-from motion photogrammetry (Turner et al., 2016) or Airborne Lidar (Stockdon et al., 2002) – typically have large uncertainties or fail in this highly dynamic and continuously wetting and drying region at the land-ocean boundary. The absence of large-scale datasets of beach face slope estimates has proved a fundamental road-block in the development of operational coastal inundation forecasting systems at the national scale (e.g., O'Grady et al., 2019) as well as in quantifying the contribution of wave run-up and setup at the shoreline relative to global sea-level rise (Melet et al., 2018; Vitousek et al., 2017). Notably, these and other studies have attempted to overcome this limitation by assuming a global-constant beach-face slope of $\tan\beta = 0.1$ (or slope-independent runup formulations), an overly-simplistic approach which has been widely criticized (e.g., Aucan et al., 2019). In this context, a new method to estimate the typical beach-face slope across large spatial scales is needed.

In this letter we present and demonstrate an innovative method to obtain estimates of the beach-face slope across the globe using satellite-derived shorelines. This approach follows recent efforts combining 30 years of satellite-derived shorelines with tidal models to create intertidal digital elevation models at the national scale (Bishop-Taylor et al., 2019a; Tseng et al., 2017). However, whereas these recent approaches obtain an approximation of the intertidal zone by assuming that the intertidal morphology at all coastal locations remains constant over time, this new approach inherently incorporates the highly dynamic nature of the intertidal zone that is observed at many sites worldwide, making it robust to the wide range of coastal environments found globally. To illustrate, Figure 1 highlights the challenges of estimating the beach-face slope at a dynamic beach where, as a result of naturally occurring cross-shore shoreline variability, a linear fit to multiple shoreline observations will always underestimate the actual steepness of the beach profile.

Following a rigorous validation of this new technique using both real and synthetic test cases ranging in slope, tidal range and wave energy, we apply the automated method across 1000's of beaches along the coastlines of eastern Australia and California, USA. We show for the first time that, at the regional scale, the distribution of beach-face slopes along these two coastlines located on opposite sides of the Pacific is very similar, with the average beach-face slope at both coastlines in the range of $\tan\beta \approx 0.06\text{-}0.07$. This new technique now paves the way to extend the analyses to the global scale.

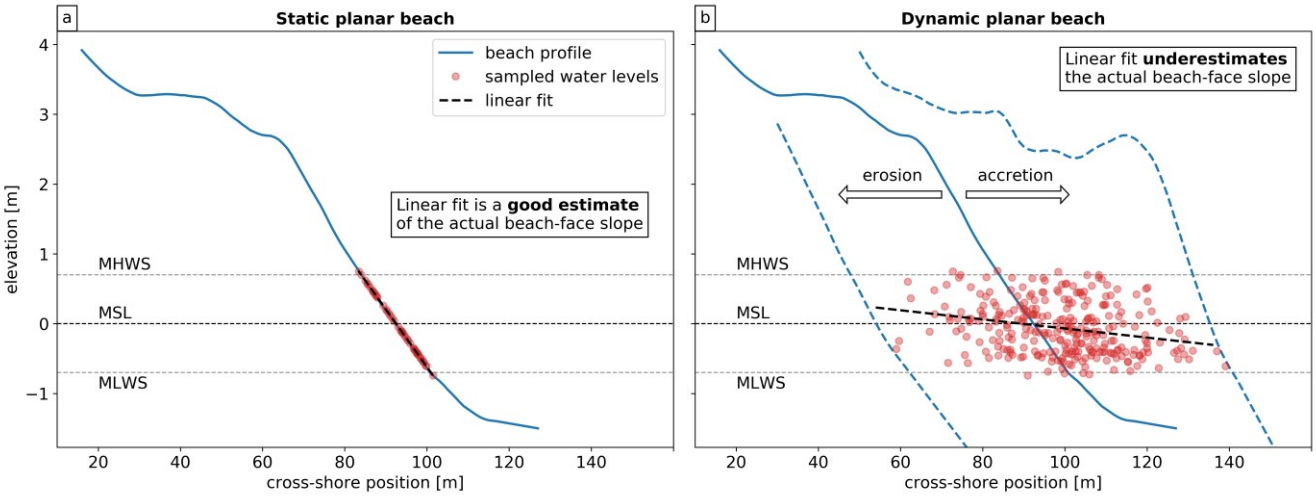


**Figure 1**. Challenges of estimating the steepness of the intertidal zone in a dynamic coastal environment where the beach face is constantly fluctuating landwards/seawards due to erosion/accretion processes. Red dots indicate long-term satellite-derived shoreline measurements (x coordinate) sampled at various tidal elevations (y coordinate). **a)** Hypothetical example of a static planar beach profile where the cross-shore variations in the water line are entirely due to the rise and fall of the tide and therefore the beach-face slope can be estimated with a simple linear fit. **b)** Real-world example of a surveyed profile at Narrabeen Beach (Australia) where the continuous erosion and accretion of the beach results in scattered observations from which the beach-face slope is significantly underestimated by a simple linear fit.

## 2 Materials and Methods

### 2.1 Test sites

To quantify and assess the capability of this novel technique to estimate beach-face slopes, eight diverse locations across three continents are considered. The selected sites exhibit a large range of beach-face slope, grain size and tidal range. Among the eight sites, two are macrotidal beaches (Slapton Sands, UK and Cable Beach, Australia), three are mesotidal beaches (Tairua, New Zealand, Torrey Pines, USA and Ensenada, Mexico), and three are microtidal beaches (Narrabeen and Moruya-Pedro, Australia and Duck, USA). The sites were selected based on availability of repeat *in situ* topographic surveys to calculate the temporal-average beach-face slope, defined for each cross-shore transect from mean sea level (MSL) to mean high water springs (MHWS). Table 1 summarises the key characteristics at each site (average beach slope, mean spring tidal range, mean deep-water significant wave height and sediment grain size) and the geographical locations are presented in Figure S1 (Supporting Information). The broad range of temporal-average beach-face slopes range from 0.025 at Cable Beach to 0.14 at Slapton Sands.

**Table 1.** Summary of the eight study sites, including average beach slope, tidal range, significant wave height (Hs) and grain size (D50). For further details on the individual sites refer to the cited publications.

| Site | Average beach-face slope [1] | Mean springs tidal range [m] | Mean deep-water $H_s$ [m] | $D_{50}$ [mm] | TR/tanβ [2] [m] | Reference publication |
|---|---|---|---|---|---|---|
| **Slapton Sands UK** | 0.14 | 4.3 | 0.5 - 1 | 2-10 | 30.7 | Ruiz de Alegria-Arzaburu and Masselink (2010) |
| **Tairua NZ** | 0.13 | 2 | 1.4 | 0.6 | 15.4 | Blossier et al. (2017) |
| **Duck USA** | 0.1 | 1.2 | 1 | 0.3 | 12 | Larson and Kraus (1994) |
| **Narrabeen AUS** | 0.09 | 1.3 | 1.6 | 0.3 | 14.4 | Turner et al. (2016b) |
| **Moruya/Pedro AUS** | 0.08 | 1.3 | 1.2 - 1.4 | 0.35 | 16.2 | Short et al. (2014) |
| **Torrey Pines USA** | 0.04 | 2.3 | 1 | 0.23 | 57.5 | Ludka et al. (2019) |
| **Ensenada MEX** | 0.03 | 2.3 | 1 | 0.25 | 76.6 | Ruiz de Alegría-Arzaburu et al. (2017) |
| **Cable Beach AUS** | 0.025 | 8.2 | NA | 0.135 | 328 | Wright et al. (1982) |

[1] beach slope is calculated between MSL and MHWS.

[2] ratio between tidal range and beach-face slope.

## 2.2 Beach-face slope estimation algorithm

The objective of the automated algorithm developed here is to estimate the beach-face slope at any site worldwide without the requirement for *in situ* measurements (e.g., topographic surveys, tide gauges, etc) but instead relying exclusively on remotely-sensed data. This new technique fully leverages the capabilities of satellite remote sensing in the coastal zone, including the use of optical imagery for mapping shoreline changes and altimetry for measuring water level changes.

Recent developments in shoreline mapping now make it possible to extract instantaneous shorelines from publicly available satellite imagery (Bishop-Taylor et al., 2019b; Pardo-Pascual et al., 2018; Vos et al., 2019a). Note that these shorelines are referred to as 'instantaneous' because they are mapped on individual satellite images acquired at different and arbitrary stages of the tide. Consequently, time-series of cross-shore change obtained from these instantaneous shorelines also implicitly include the superposition of tidal excursion and sediment transport processes – i.e., beach erosion/accretion. In order to estimate the slope of the beach face, the fluctuations caused by tidal excursions must be isolated from the horizontal changes resulting from erosion and/or accretion of the beach. To do this we use a frequency-domain analysis to isolate the high-frequency tidal signal in the cross-shore shoreline time-series from the typically lower-frequency morphological changes. The step-by-step methodology to estimate the typical beach-face slope from satellite-derived shorelines and modelled tide levels is illustrated in Figure 2 and described below.

*1) Extract satellite-derived shorelines from Landsat imagery (Figure 2a):*

Satellite-derived instantaneous shorelines are extracted using *CoastSat* (Vos et al., 2019a), an open-source toolbox that enables users to obtain time-series of cross-shore shoreline position at any sandy coastline worldwide from 30+ years of publicly available satellite imagery (Landsat 5, 7, 8 and Sentinel-2) accessed via Google Earth Engine (Gorelick et al., 2017). A target sampling period of no more than 8 days was maintained by the use of all Landsat images between 1999 and 2019 (i.e., 16-day revisit with at least 2 satellites concurrently in orbit). Sentinel-2 images were excluded as the poor cloud masking algorithm hampered a fully automated shoreline extraction. The cross-shore accuracy of the mapped shorelines varies between 10 and 15 m depending on site characteristics, as was previously reported in Vos et al. (2019b). Time-series of cross-shore shoreline change were obtained by intersecting the mapped shorelines with shore-normal transects at each site. An example of the resulting raw time-series of shoreline change at Cable Beach is shown in Figure 2a.

*2) Tide levels from a global tide model and peak tidal frequency (Figures 2b and 2d):*

Once the satellite-derived shorelines have been mapped, the corresponding tide levels at the time of image acquisition are obtained from the FES2014 global tide model (Carrere et al., 2016). This model was chosen as it ranks amongst the best barotropic ocean tide models for coastal regions (Stammer et al., 2014). The next step is to identify in the tide elevation time-series (sub-sampled according to availability of satellite-derived shorelines) the frequency at which the tidal signal is the strongest. This frequency, hereafter referred to as 'peak tidal frequency', is determined by computing the Power Spectrum Density (PSD) of the tide level time-series. Importantly, the PSD cannot be computed with a traditional Fourier Transform (e.g., FFT) as the tide level time-series are unevenly sampled due to the presence of clouds within the associated satellite images. However an alternative algorithm, the Lomb-Scargle transform (VanderPlas, 2018), widely used to analyse astronomical observations, is specifically suited to the calculation of the PSD from irregularly sampled time-series (see comparison with FFT in Supporting Information Figure S2).

The PSD of the tidal signal, depicted in Figure 2d, indicates how much tidal energy is contained at a given frequency, with the peaks revealing the frequency of the tidal harmonic constituents. Since the tide is sub-sampled at 8-day intervals, the higher-frequency semi-diurnal and diurnal components of the tide are completely missed, but some of the lower-frequency components can be resolved (e.g., *Msf* lunisolar synodic fortnightly, *Sa* annual). Figure 2d shows the PSD of the sub-sampled tide time-series, indicating that the highest peak is located at a period of 17.5 days. This energy corresponds to the lunisolar synodic fortnightly component (*Msf*), which has a period of 14.76 days, but as the *Nyquist limit* is 16 days (twice the sampling period), the 14.76 days periodic signal is slightly aliased to 17.5 days. The aliasing of the tidal signal and the effect of the sampling frequency are further discussed in Supporting Information S3.

*3) Tidal correction with a range of beach-face slope values (Figure 2c):*

Tidal correction consists of the projection of individual instantaneous shorelines, acquired at different stages of the tide, to a standard reference elevation, for example Mean Sea Level (MSL).

A simple tidal correction is applied by translating horizontally the shoreline points along a cross-shore transect using a linear slope:

$$\Delta x_{corrected} = \Delta x + \frac{z_{tide}}{tan\beta} \quad (1)$$

Where $\Delta x_{corrected}$ is the tidally-corrected cross-shore position, $\Delta x$ is the instantaneous cross-shore position, $z_{tide}$ is the corresponding tide level and $tan\beta$ is the beach-face slope. Using Eq. (1) the raw time-series of cross-shore shoreline positions were tidally corrected using a range of potential slope values from 0.01 to 0.2, which is considered "a universally relevant upper limit of sandy beach-face slopes" (Bujan et al., 2019).

*4) Find the slope that minimises the tidal component of the shoreline time-series (Figures 2e and 2f):*

As the final step in this automated process, the Lomb-Scargle transform is employed to compute the PSD of each of the tidally-corrected time-series. Figure 2e shows the PSD curves resulting from the tidally-corrected time-series depicted In Figure 2c. An inset on the peak tidal frequency band (17.5 days) demonstrates how the magnitude of this peak is modulated by the slope value used for tidal correction. In this example (Cable Beach), the 17.5 days peak is entirely suppressed when using a slope of 0.025 (as indicated by the blue dashed curve).

Finally, the typical beach-face slope can be estimated by finding the slope value that, when used to tidally-correct the shoreline time-series, minimises the amount of tidal energy. Figure 2f shows the 'tidal energy' (i.e., the integral of PSD inside the peak tidal frequency band) as a function of the slope value used for tidal correction, indicating a distinct minimum for a slope of 0.025. For this site, this leads to the conclusion that tanβ = 0.025 is the temporal-average beach-face slope at this macro-tidal, fine sand grain size location.

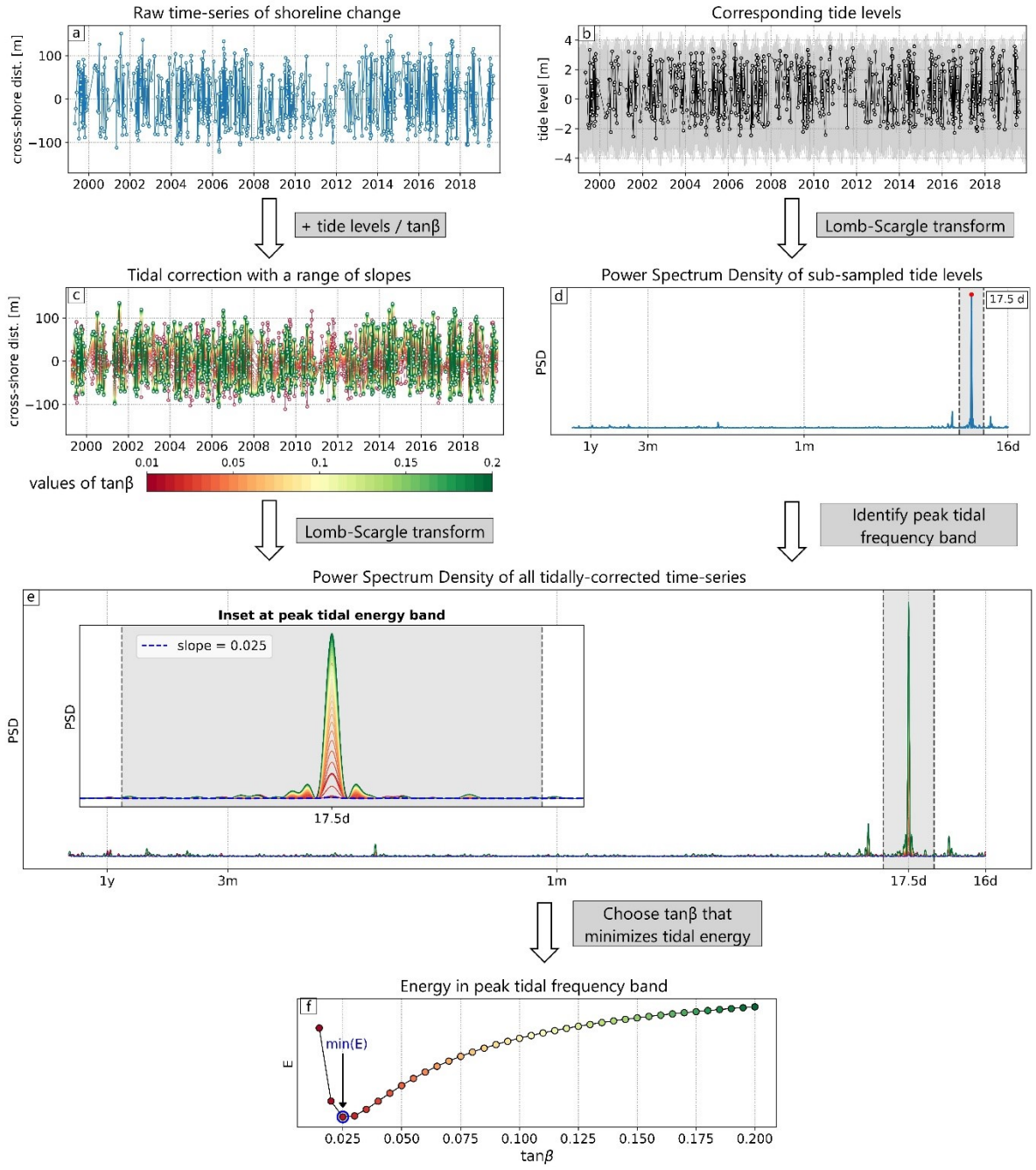


**Figure 2**. Step-by-step description of the algorithm developed to estimate typical beach-face slope from satellite-derived shorelines. The time-series of shoreline change and tide levels shown here are from Cable Beach (Western Australia). **a)** Raw (i.e., non-tidally corrected) time-series of shoreline change along the southern shore-normal transect at Cable Beach (see Figure S1 in Supporting Information). **b)** Modelled tide levels associated with the satellite-derived shorelines (black line). The grey shaded area indicates the overall tidal fluctuations. **c)** Ensemble of tidally-corrected time-series of shoreline change using slope values ranging from 0.01 (red) to 0.2 (green). **d)** Power Spectrum Density (PSD) of the sub-sampled tide level time-series. The peak tidal frequency band (grey shaded area) is centred at a frequency of 17.5 days and stretches $10^{-8}$ Hz each side. **e)** PSD of the ensemble of tidally-corrected shoreline time-series. The inset

zooms on the peak tidal frequency band and shows how the magnitude of the peak at this frequency is entirely suppressed when using a slope of 0.025 (blue dashed line). **f)** Energy in the peak tidal frequency band for the range of slopes tested. The slope that minimises the energy inside the peak tidal frequency band is selected as the best estimate of the beach-face slope.

## 3 Results

The beach-face slope estimation algorithm described in the previous section was applied to the eight test sites along the transects depicted in Figure S1 (39 transects in total) and compared to *in situ* measurements. The measured beach-face slope at each transect was computed as the average of all the available surveys (calculated from MSL to MHWS), except at Cable Beach where only one known survey was conducted (Wright et al., 1982). Figure 3a shows a 1:1 plot comparing the satellite-derived beach-face slopes ($\tan\beta_{satellite}$) to the *in situ* beach-face slopes ($\tan\beta_{in\ situ}$). For the *in situ* data (x-axis), a horizontal bar indicates one standard deviation around the average to highlight the degree of temporal variability in beach-face slope observed at each location.

Overall, there is a strong correlation between satellite-derived estimates and *in situ* averages, with a coefficient of determination ($R^2$) of 0.93 and no systematic under- or over-estimation observed. While the slope estimation algorithm performed very well along the gentle sloping profiles ($\tan\beta_{in\ situ} < 0.05$) of Cable Beach, Ensenada and Torrey Pines, as well as along the steeper ($\tan\beta_{in\ situ} > 0.12$) profiles at Slapton Sands and Tairua, relatively more scatter is observed at the more intermediate sites (Duck, Moruya/Pedro and Narrabeen). These intermediate sites ($0.5 < \tan\beta_{in\ situ} < 0.12$) are also characterised by a larger temporal variability in beach slope as indicated by the width of the standard deviation bars. In terms of accuracy, the standard deviation of the errors was 0.01 with 90% of the errors falling below 0.015.

While this new capability may become highly valuable for a range of applications as it does not rely on any field measurements, there are limitations. Firstly, this method relies on the existence of a measurable tidal excursion signal in the satellite-derived shoreline time-series. Since the horizontal accuracy of the satellite-derived shorelines is ~10m, in order to capture the tidal excursion signal, the amplitude of this fluctuation needs to be significantly larger than 10m – e.g., a tidal excursion of 20 m has a signal-to-noise ratio of 2. In turn, the amplitude of the tidal excursion depends on the tidal range and on the angle of the intertidal zone.

To identify the range of tidal regimes and beach-face slopes over which this method is applicable, additional synthetic time-series of shoreline change were generated for a planar beach with specified slope and tidal range (the details on how these time-series were generated are included in Supporting Information S4). Figure 3b summarises the accuracy of the estimated beach-face slopes - i.e., Normalised Mean Absolute Error (MNAE) based on 100 synthetic time-series - as a function of tidal range (TR) and beach-face slope ($\tan\beta$). As anticipated, the accuracy declines with decreasing tidal range and increasing beach-face slope, as a decrease in the ratio TR/$\tan\beta$ is equivalent to reducing the amplitude of the horizontal tidal excursions. Based on these synthetic data, the errors can be as much as 30% for TR/$\tan\beta$ ratios smaller than 10 (i.e., TR < 1 m and $\tan\beta$

> 0.1). Consequently, in order to obtain accurate slope estimates, it is recommended that the technique be applied at any site where TR/tanβ is larger than 10. This is further emphasised by the fact that every one of the eight test sites, for which the tidal ranges and average *in situ* beach-face slopes are also included in Figure 3b, are situated at locations where TR/tanβ > 10 (exact ratios reported in Table 1).

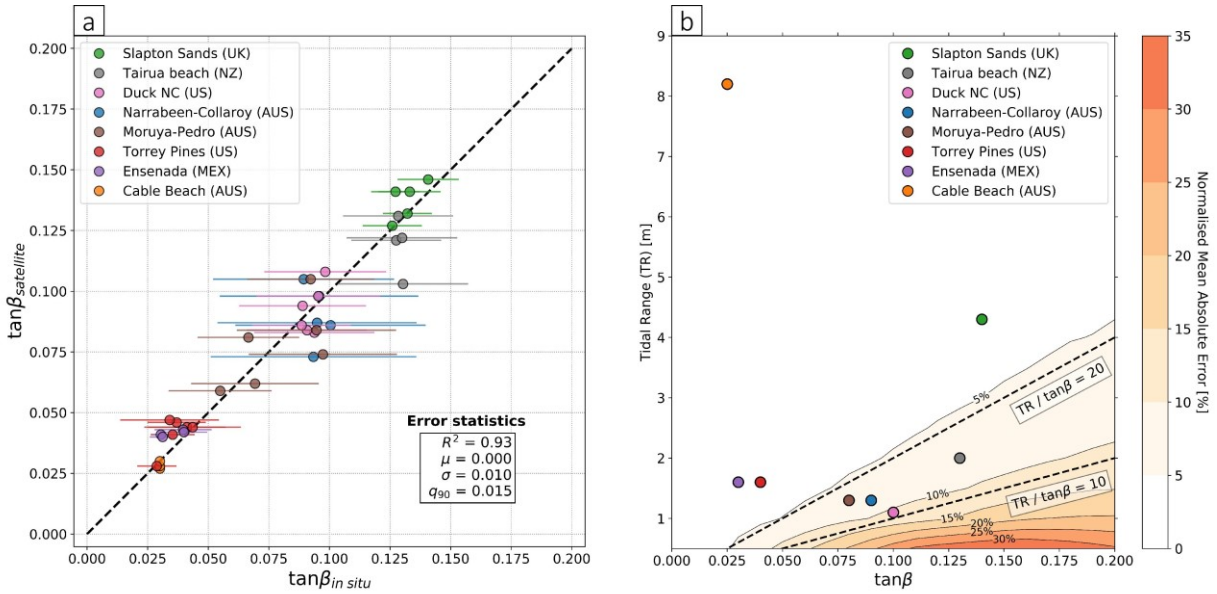


**Figure 3**. Quantitative assessment of the beach-face slope estimation technique. **a)** 1:1 plot illustrating the comparison between *in situ* measurements of the beach-face slope (x-axis) and satellite-derived estimates (y-axis) at the eight test sites (total of 39 cross-shore transects). The horizontal bars represent one standard deviation from the average *in situ* slope and indicate the degree of temporal variability in beach-face slope at each transect. **b)** Synthetic analysis showing that the accuracy of the method declines with decreasing tidal range to beach-face slope ratio TR/tanβ. The orange contours represent the Normalised Mean Absolute Error (NMSE) for each combination of tidal range and beach-face slope based on 100 synthetic shoreline time-series (described in Supporting Information S4). The two black dashed lines indicate respectively a ratio of tidal range to beach-face slope of 10 and 20. The dots indicate the tidal range and average beach-face slope at each of the eight test sites.

## 4 Regional-scale application: Eastern Australia and California USA coastlines

To demonstrate how this technique can be applied over large spatial scales, an example application at the regional scale along two stretches of coastline is presented here: the south-eastern Australian coastline (~1800 km) and the California USA coast (~1500km). The methodology described in Section 2 was applied at 100 m alongshore-spaced intervals at sandy beaches along both coasts; in eastern Australia this resulted in a total of 13,624 beach-face slope estimates; in California 8,147. The results are shown in Figures 4a and 4b and the complete dataset is available as an interactive web dashboard in the Data Availability section below. The regional-scale distributions of beach-face slopes are depicted in Figure 4c, and intriguingly, they appear to be very similar. In both

eastern Australia and California approximately 80% of time-averaged slopes are between 0.04 and 0.08, with the corresponding means of 0.062 (SE Australia) and 0.068 (California).

As a pointer to where the new availability of broad-scale beach slope information may find further application, an empirical relationship between beach-face slope and sediment size $D_{50}$ was recently derived by Bujan et al. (2019) based on 2,144 individual field measurements. This equation can now be employed along the south-eastern Australian and Californian coastlines to convert the beach-face slope estimates to the equivalent grain size ($D_{50}$) and obtain an estimate of the distribution of sediment grain sizes for beaches occurring along the full extent of both regions (see inset in Figure 4c). The detailed analyses of beach-face slope and sediment size distributions at regional scales are outside the scope of this letter, but this example demonstrates the significant potential of this technique to provide beach-face slope estimates as well as sediment size distributions at the global scale.

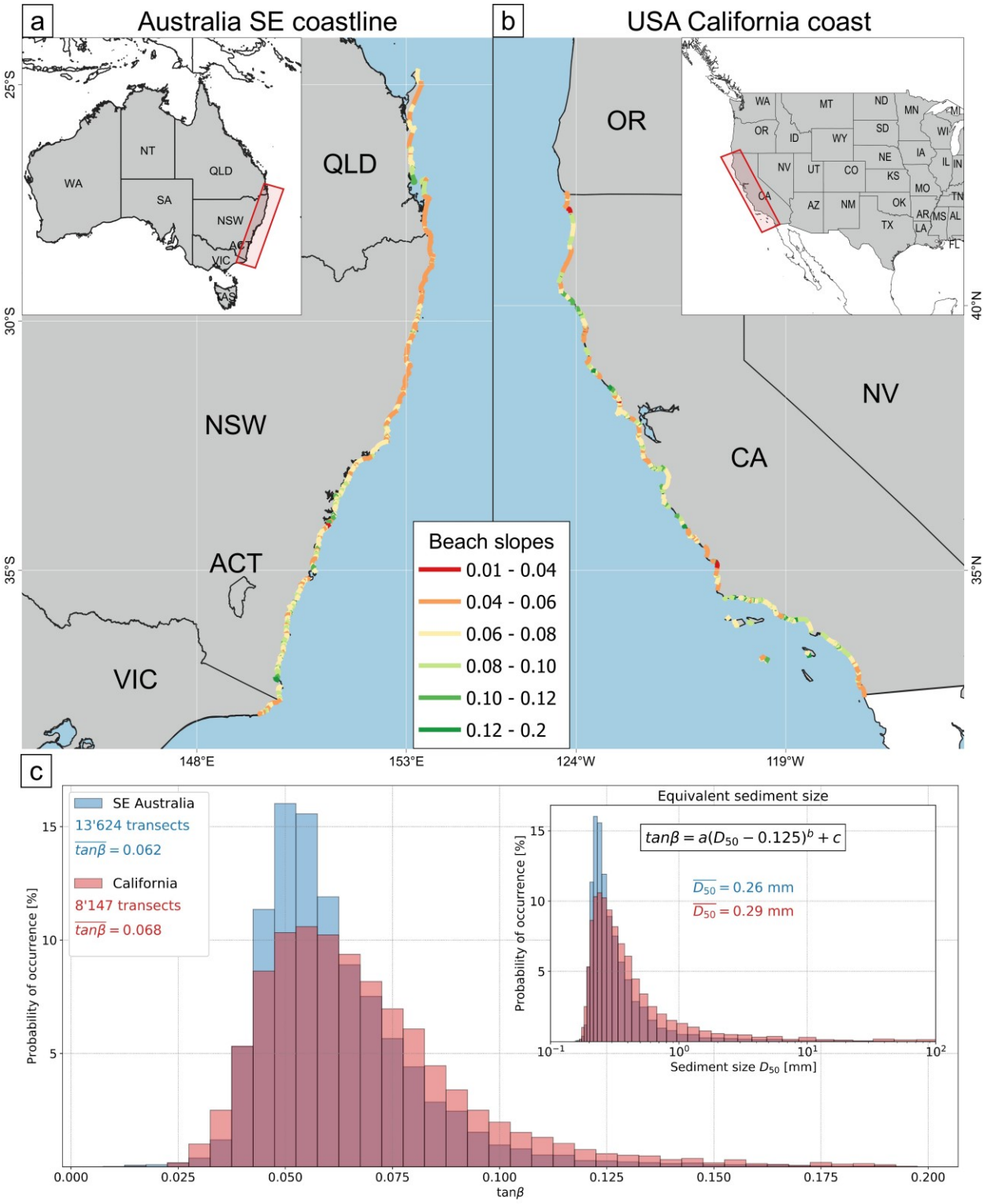


**Figure 4**. Regional-scale application over SE Australia and California. The mean beach-face slope is 0.062 for SE Australia and 0.068 for California, with both regions showing similar distributions around the mean. **a)** Map of beach-face slopes estimated along 13'624 transects on the SE Australian coastline. **b)** Map of beach-face slopes estimated along 8'147 transects on Californian US west coast. **c)** Histogram of the distribution of beach-face slopes along the two stretches of coastline (SE Australia and California). In the

top-right inset the equivalent sediment size distributions are obtained with the empirical relationship from Bujan et al. (2019). The mean $D_{50}$ values are 0.26 and 0.29 mm respectively for SE Australia and California.

## 5 Conclusions

A novel methodology to estimate beach-face slopes from satellite-derived shorelines and modelled tides is described here and evaluated along eight diverse sandy/gravel beaches spanning a broad range of tidal regimes, beach-face slopes and wave climates. This new technique employs a variant of the Fourier transform, the Lomb-Scargle transform, to identify the slope that, when used for tidal correction, minimises the tidal energy in the shoreline time-series.

A comparison with *in situ* (beach survey) topographic data along 39 transects demonstrates that this technique is capable of estimating the time-averaged beach-face slope in different coastal environments ranging from macrotidal, gentle-sloping beaches, to microtidal wave-dominated beaches. Further analysis using synthetic shoreline data reveals that the accuracy of this method declines significantly when the ratio between tidal range and beach-face slope is < 10.

Finally, an example application spanning a section of the Eastern Australia and California USA coastlines demonstrates the capability of this technique to estimate beach-face slopes over large spatial scales, with the potential to now create and further investigate a global dataset of beach-face slopes. It is anticipated that the future availability of such a dataset will be a key variable to support global studies on the impact of sea level rise and increased storminess along world coastlines.

## Acknowledgments

The authors would like to thank the multiple individuals and organisations that made available the *in situ* beach slope data used for validation in this study: Slapton Sands (UK) beach surveys were obtained from the Channel Coastal Observatory (https://www.channelcoast.org); Funding for the routine monitoring at Narrabeen is provided by Northern Beaches Council, UNSW Research Infrastructure Scheme, UNSW Faculty of Engineering Early Career Grant, the NSW Adaptation Research Hub – Coastal Processes Node (Office of Environment and Heritage), and the Australian Research Council (LP0455157, LP100200348, DP150101339, LP170100161); Prof. A.D. Short (Univ. of Sydney) provided the surveyed profiles at Moruya and Pedro beaches; Jennifer Montano Munoz (Univ. of Auckland) and Chris kindly provided the surveyed data for Tairua beach (New Zealand); Torrey-Pines (California) survey data was compiled and made publicly available by the Scripps Institution of Oceanography in Ludka et al. (2019); special thanks to Amaia Ruiz de Alegria Arzaburu and Jesus Adrian Vidal Ruiz from the Autonomous University of Baja California who generously shared beach slope data for Ensenada beach, Mexico; the Duck (North Carolina) data set is maintained by the U.S. Army Engineer Research & Development Centre, Coast & Hydraulics Laboratory, Field Research Facility. Finally, FES2014 was produced by Noveltis, LEGOS and CLS and distributed by AVISO+ (https://www.aviso.altimetry.fr) with support from CNES (French National Centre for Space Studies). In particular, the authors wish to acknowledge

Frederic Briol for developing the Python wrapper to FES2014, a fantastic tool for end users. Thanks also to Sean Vitousek for his insightful comments and suggestions. The lead author is supported by a UNSW Scientia PhD scholarship.

## Data availability

The beach-face slope datasets for the SE Australia and California coastlines have been uploaded in the following open-access Zenodo data repository https://doi.org/10.5281/zenodo.3747130 and can also be visualised and downloaded on an interactive web dashboard at http://coastsat.wrl.unsw.edu.au/.

## References

Aucan, J., Hoeke, R. K., Storlazzi, C. D., Stopa, J., Wandres, M., & Lowe, R. (2019). Waves do not contribute to global sea-level rise. *Nature Climate Change*, *9*(1), 2–2. https://doi.org/10.1038/s41558-018-0377-5

Battjes, J. A. (1974). Surf similarity, paper presented at 14th International Conference on Coastal Engineering. *Am. Soc. of Civ. Eng., Copenhagen*.

Bishop-Taylor, R., Sagar, S., Lymburner, L., & Beaman, R. J. (2019). Between the tides: Modelling the elevation of Australia's exposed intertidal zone at continental scale. *Estuarine, Coastal and Shelf Science*, *223*(October 2018), 115–128. https://doi.org/10.1016/j.ecss.2019.03.006

Bishop-Taylor, R., Sagar, S., Lymburner, L., Alam, I., & Sixsmith, J. (2019). Sub-pixel waterline extraction: Characterising accuracy and sensitivity to indices and spectra. *Remote Sensing*, *11*(24), 1–23. https://doi.org/10.3390/rs11242984

Blossier, B., Bryan, K. R., Daly, C. J., & Winter, C. (2017). Shore and bar cross-shore migration, rotation, and breathing processes at an embayed beach. *Journal of Geophysical Research: Earth Surface*, *122*(10), 1745–1770. https://doi.org/10.1002/2017JF004227

Bujan, N., Cox, R., & Masselink, G. (2019). From fine sand to boulders: examining the relationship between beach-face slope and sediment size. *Marine Geology*, 106012. https://doi.org/10.1016/j.margeo.2019.106012

Carrere, L., Lyard, F., Cancet, M., Guillot, A., & Picot, N. (2016). FES 2014, a new tidal model—Validation results and perspectives for improvements. In *Proceedings of the ESA living planet symposium* (pp. 9–13). https://doi.org/https://www.aviso.altimetry.fr/

Gorelick, N., Hancher, M., Dixon, M., Ilyushchenko, S., Thau, D., & Moore, R. (2017). Google Earth Engine: Planetary-scale geospatial analysis for everyone. *Remote Sensing of Environment*, *202*, 18–27. https://doi.org/10.1016/j.rse.2017.06.031

Harley, M. D., Turner, I. L., & Short, A. D. (2015). New insights into embayed beach rotation: The importance of wave exposure and cross-shore processes. *Journal of Geophysical Research F: Earth Surface*, *120*(8), 1470–1484. https://doi.org/10.1002/2014JF003390

Larson, M., & Kraus, N. C. (1994). Temporal and spatial scales of beach profile change, Duck, North Carolina. *Marine Geology*, *117*(1–4), 75–94. https://doi.org/10.1016/0025-3227(94)90007-8

Ludka, B. C., Guza, R. T., O'Reilly, W. C., Merrifield, M. A., Flick, R. E., Bak, A. S., et al. (2019). Sixteen years of bathymetry and waves at San Diego Beaches. *Scientific Data*, *6*(1), 161. https://doi.org/10.1038/s41597-019-0167-6

Melet, A., Meyssignac, B., Almar, R., & Le Cozannet, G. (2018). Under-estimated wave contribution to coastal sea-level rise. *Nature Climate Change*, *8*(3), 234–239. https://doi.org/10.1038/s41558-018-0088-y

O'Grady, J. G., McInnes, K. L., Hemer, M. A., Hoeke, R. K., Stephenson, A. G., & Colberg, F. (2019). Extreme Water Levels for Australian Beaches Using Empirical Equations for Shoreline Wave Setup. *Journal of Geophysical Research: Oceans*, *124*(8), 5468–5484. https://doi.org/10.1029/2018jc014871

Pardo-Pascual, J. E., Sánchez-García, E., Almonacid-Caballer, J., Palomar-Vázquez, J. M., de los Santos, E. P., Fernández-Sarría, A., & Balaguer-Beser, Á. (2018). Assessing the accuracy of automatically extracted shorelines on microtidal beaches from landsat 7, landsat 8 and sentinel-2 imagery. *Remote Sensing*, *10*(2). https://doi.org/10.3390/rs10020326

Parker, B. B. (2007). *Tidal analysis and prediction*. Silver Spring, MD, NOAA NOS Center for Operational Oceanographic Products and Services. https://doi.org/http://dx.doi.org/10.25607/OBP-191

Ruiz de Alegria-Arzaburu, A., & Masselink, G. (2010). Storm response and beach rotation on a gravel beach, Slapton Sands, U.K. *Marine Geology*, *278*(1–4), 77–99. https://doi.org/10.1016/j.margeo.2010.09.004

Ruiz de Alegría-Arzaburu, A., Vidal-Ruiz, J. A., García-Nava, H., & Romero-Arteaga, A. (2017). Seasonal morphodynamics of the subaerial and subtidal sections of an intermediate and mesotidal beach. *Geomorphology*, *295*(June), 383–392. https://doi.org/10.1016/j.geomorph.2017.07.021

Senechal, N., Coco, G., Bryan, K. R., & Holman, R. A. (2011). Wave runup during extreme storm conditions. *Journal of Geophysical Research: Oceans*, *116*(7), C07032. https://doi.org/10.1029/2010JC006819

Short, A. D., Williamson, B., & Hogan, C. L. (1993). The Australian Beach Safety and Management Program - Surf Life Saving Australia's Approach to Beach Safety and Coastal Planning. *11th Australasian Conference on Coastal and Ocean Engineering (Townsville, Qld.)*, *National c*(93/4), 113–118. Retrieved from https://search.informit.com.au/documentSummary;dn=560087890263399;res=IELENG

Short, A. D., Bracs, M. A., & Turner, I. L. (2014). Beach oscillation and rotation: local and regional response at three beaches in southeast Australia. *Journal of Coastal Research*, (Special Issue 66), 712–717. https://doi.org/10.2112/SI65-xxx.1

Stammer, D., Ray, R. D., Andersen, O. B., Arbic, B. K., Bosch, W., Carrère, L., et al. (2014, September 1). Accuracy assessment of global barotropic ocean tide models. *Reviews of Geophysics*. Blackwell Publishing Ltd. https://doi.org/10.1002/2014RG000450

Stephens, S. A., Coco, G., & Bryan, K. R. (2011). Numerical Simulations of Wave Setup over Barred Beach Profiles: Implications for Predictability. https://doi.org/10.1061/(ASCE)WW.1943-5460.0000076

Stockdon, H.F., Asbury H., Jr., S., List, J. H., & Holman, R. A. (2002). Estimation of Shoreline Position and Change Using Airborne Topographic Lidar Data. *Journal of Coastal Research*, *18*(3), 502–513. https://doi.org/10.2307/4299097

Stockdon, Hilary F., Holman, R. A., Howd, P. A., & Sallenger, A. H. (2006). Empirical parameterization of setup, swash, and runup. *Coastal Engineering*, *53*(7), 573–588. https://doi.org/10.1016/j.coastaleng.2005.12.005

Stockdon, Hilary F., Sallenger, A. H., Holman, R. A., & Howd, P. A. (2007). A simple model for the spatially-variable coastal response to hurricanes. *Marine Geology*, *238*(14), 1–20. https://doi.org/10.1016/j.margeo.2006.11.004

Tseng, K. H., Kuo, C. Y., Lin, T. H., Huang, Z. C., Lin, Y. C., Liao, W. H., & Chen, C. F. (2017). Reconstruction of time-varying tidal flat topography using optical remote sensing imageries. *ISPRS Journal of Photogrammetry and Remote Sensing*, *131*, 92–103. https://doi.org/10.1016/j.isprsjprs.2017.07.008

Turner, I. L., Harley, M. D., Short, A. D., Simmons, J. A., Bracs, M. A., Phillips, M. S., & Splinter, K. D. (2016). A multi-decade dataset of monthly beach profile surveys and inshore wave forcing at Narrabeen, Australia. *Scientific Data*, *3*, 160024. https://doi.org/10.1038/sdata.2016.24

Turner, I. L., Harley, M. D., & Drummond, C. D. (2016). UAVs for coastal surveying. *Coastal Engineering*, *114*, 19–24. https://doi.org/10.1016/j.coastaleng.2016.03.011

VanderPlas, J. T. (2018). Understanding the Lomb–Scargle Periodogram. *The Astrophysical Journal Supplement Series*, *236*(1), 16. https://doi.org/10.3847/1538-4365/aab766

Vitousek, S., Barnard, P. L., Fletcher, C. H., Frazer, N., Erikson, L., & Storlazzi, C. D. (2017). Doubling of coastal flooding frequency within decades due to sea-level rise. *Scientific Reports*, *7*(1), 1–9. https://doi.org/10.1038/s41598-017-01362-7

Vos, K., Splinter, K. D., Harley, M. D., Simmons, J. A., & Turner, I. L. (2019). CoastSat: A Google Earth Engine-enabled Python toolkit to extract shorelines from publicly available satellite imagery. *Environmental Modelling & Software*, *122*, 104528. https://doi.org/10.1016/j.envsoft.2019.104528

Vos, K., Harley, M. D., Splinter, K. D., Simmons, J. A., & Turner, I. L. (2019). Sub-annual to multi-decadal shoreline variability from publicly available satellite imagery. *Coastal Engineering*, *150*, 160–174. https://doi.org/10.1016/j.coastaleng.2019.04.004

Wright, L. D., Nielsen, P., Short, A. D., & Green, M. O. (1982). Morphodynamics of a macrotidal beach. *Marine Geology*, *50*.

.